TÜBİTAK

Turkish Journal of Electrical Engineering & Computer Sciences

http://journals.tubitak.gov.tr/elektrik/

Research Article

Turk J Elec Eng & Comp Sci
(2013) 21: 1107 – 1119

doi:10.3906/elk-1110-67

Linear switched reluctance motor control with PIC18F452 microcontroller

Mahir DURSUN,[1,*] **Fatmagül KOÇ**[2]

[1]Department of Electrical and Electronic Engineering, Technology Faculty, Gazi University, 06500 Teknikokullar, Ankara, Turkey

[2]Department of Electrical and Energy Engineering, Gazi Vocational High School, Gazi University, 06500 Çubuk, Ankara, Turkey

Received: 30.10.2011 • **Accepted:** 24.03.2012 • **Published Online:** 03.06.2013 • **Printed:** 24.06.2013

Abstract: This paper presents the simulation, control, and experimental results of the velocity of a double-sided, 6/4-poled, 3-phased, 8 A, 24 V, 250 W, and 250 N pull force linear switched reluctance motor (LSRM). In the simulation and experimental study, the reference velocity is constant depending on the position and time. The velocity versus the position of the translator was controlled with fuzzy logic control (FLC) and proportional-integral (PI) control techniques. The motor was controlled by PI control method with a PIC18F452 microcontroller due to its low cost. The results of the velocity of a translator were compared with the simulation results of the PI control and FLC techniques. It was seen that the PIC18F452 microcontroller is sufficient in the velocity control of the LSRM, and in the FLC method, the force and velocity ripples are lower than in the PI control method.

Key words: Linear switched reluctance motor, LSRM control, fuzzy logic control, proportional-integral control, velocity control

1. Introduction

Linear motion with rotary motors and linear mechanical interfaces causes a backlash due to gears and problems such as hysteresis [1]. Linear motors eliminate the need for rotary-to-linear mechanical interfaces, resulting in a simpler and more robust conversion of the electrical input into a linear motion. In addition, these motors are quiet and reliable and have so far been successfully applied in conveyor systems, people movers, sliding doors, and airport baggage handling, to mention a few [2].

Linear switch reluctance motors (LSRMs) have the same advantages as other linear motors. Moreover, the LSRM has a simple structure that is sturdy, reliable, and low-cost. It is also adaptable to harsh environments and can be controlled easily in terms of position and velocity. Therefore, the LSRM is an attractive candidate for position and velocity control [3]. Unfortunately, the sufficient and widespread use of motors in industrial applications has not yet been seen, because of the unknown characteristics of these motors and because the drivers and controllers' specifications are insufficient.

The LSRM is a new kind of linear traction motor that has been developed based on the study of the switched reluctance motor (SRM) [3] and combines the advantages of the SRM and the traditional linear motor [4]. The LSRM has 2 major characteristics: first, the mover of the LSRM is connected directly to the load without any traditional rotary-to-linear mechanical translator, which reduces loss and lowers system costs, and second, the motor windings are connected to the switching circuit, which uses the modern power electronic

*Correspondence: mdursun@gazi.edu.tr

technique. Thus, the LSRM has a large starting moment, high overload capacity, wide speed range, and other advantages. Compared with other AC linear motors, the LSRM has extensive application prospects in high-precision processing and high-power transmission.

In the literature, there are some studies about the determination of the geometric dimensions of a double-sided LSRM, the velocity and position control with fuzzy logic, and the elevator application of the LSRM [5–8]. Dursun applied a 3-phase fuzzy logic-controlled SRM to a wheelchair drive with a speed controller in his study [9]. In 2007, Liu et al. presented the design and analysis of a longitudinal flux LSRM for high-precision position control applications [10]. In 2008, Lim and Krishnan presented a LSRM in which the primary propulsion of a ship elevator was proposed and investigated [2]. Similar studies are encountered in the literature and SRM control [11–29].

In this study, to achieve the low cost and efficiency of a driver in linear motions, first, a double-sided, 6/4-poled, 3-phased, 8 A, 24 V, 250 W LSRM, having a 250 N pull force, was used in locations where a linearly moving accurate position, easy control, and rapid response are requested. The LSRM's operation and switching sections as the motor and generator are determined and the fuzzy logic and proportional-integral (PI) control method velocity and position control were simulated. In the simulation and experimental study, the reference velocity is constant, depending on the position and time. The velocity of the translator versus the position by the fuzzy logic control (FLC) and PI control techniques was examined. The motor was controlled with a PIC18F452 microcontroller due to its low cost. The results of the velocity of the translator were compared with the simulation results of the PI and FLC techniques. It was seen that the PIC18F452 microcontroller is sufficient in the velocity control of the LSRM, and in the FLC method, the force and velocity ripples are lower than in the PI control method.

2. Analysis of motor

2.1. Numerical analysis of motor

The ideal inductance profile was driven against the translator position of the designed motor. The minimum phase inductance value of the motor is indicated as 0.002 mH and the maximum value of the phase inductance is indicated as 0.012 mH for 8 A.

The electrical properties of the motor are determined as 250 W, 24 V DC, and 8 A. All of the motor parameters are given in the Table.

Table. Data sheet of the calculated design parameters.

Symbol	Design parameter	Value
L	Length of the LSRM	0.8 m
v_m	Maximum linear velocity	1 m/s
t_a	Acceleration time	0.167 s
m	Mass for translator	25 kg
F	Pull force	250 N
P	Power of the LSRM	250 W
I	Current	8 A

The appropriate mechanical and electrical parameters were designed and the motor was visualized as 3-dimensional (3D). Based on these parameters, the 3D figure of the motor was drawn with computer-aided design software and is shown in Figure 1. The induced electromagnetic force, magnetic flux and magnetic

flux with the flux density, and magnetic flux with the flux density vectors, were obtained for this design. The obtained values are nonlinear functions because they are changed according to the locations of the rotor and flux. The variables in the magnetic analyses of the motor are the location of the armature and winding currents. The software composes the finite element surface of the motor, depending upon the location of the armature, and then calculates the basic outlet parameters, such as the phase inductions.

During the magnetic analyzing of the designed motor, an 8 A current was applied. In this case, the force obtained in the state of armature is shown as the force in Figure 2. The graph in Figure 2 shows the force alteration of the stator and armature from the total detached status to the coincident status. The phase's inductance changes versus the positions and currents is given in Figure 3.

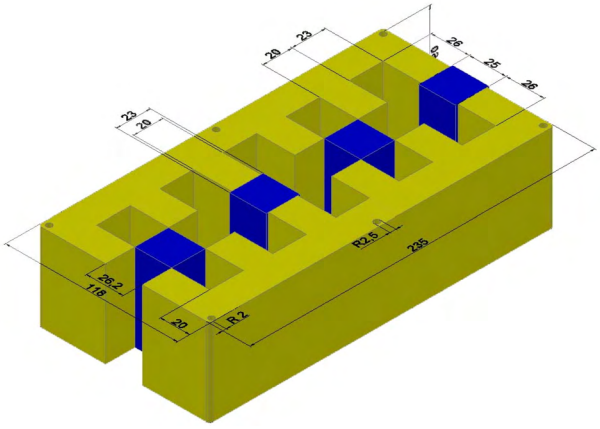

Figure 1. 3D model of the LSRM.

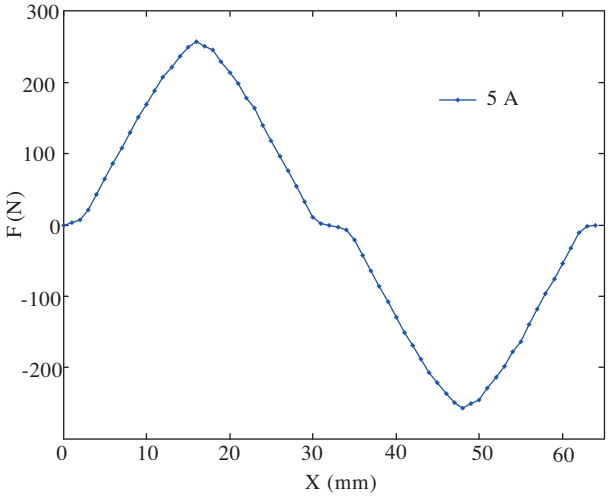

Figure 2. Translator position–force change.

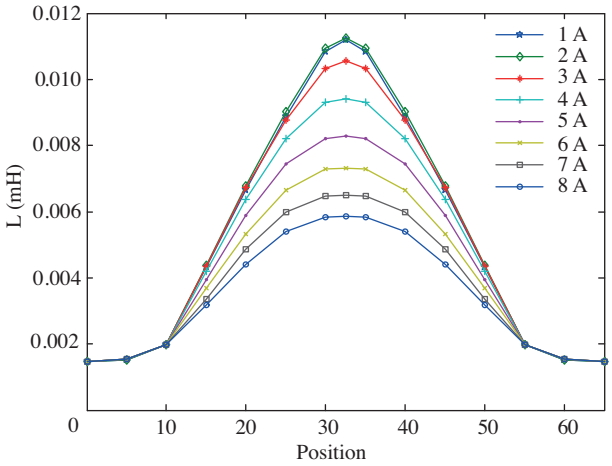

Figure 3. The inductance change versus the positions and currents.

3. Dynamic analysis of the LSRM

In order to establish a realistic model of the SRM, it is necessary to know all of the relevant parameters. The total magnetic flux vector of the motor $\lambda^T = \begin{bmatrix} \lambda_1 & \lambda_2 & \lambda_3 \end{bmatrix}$ is as follows:

$$\lambda = L(x)i, \tag{1}$$

where the current vector, $i^T = \begin{bmatrix} i_a & i_b & i_c \end{bmatrix}$, includes the phase currents, x is the position of the slider, and the inductance matrix $L(x)$ is given as:

$$L(x) = \begin{bmatrix} L_{aa} & L_{ab} & L_{ac} \\ L_{ba} & L_{bb} & L_{cc} \\ L_{ca} & L_{cb} & L_{cc} \end{bmatrix}. \tag{2}$$

From the electromagnetic energy conversion theory, the voltage equation of the motor could be written as:

$$V = Ri + L(x)\frac{di}{dt} + v\frac{dL(x)}{dx}i, \tag{3}$$

where v is the velocity of the slider, the voltage vector $V^T = \begin{bmatrix} v_a & v_b & v_c \end{bmatrix}$ contains the supply voltage for each phase, and V is the same in all of the phases. Moreover, the resistance matrix could be given as:

$$R = \begin{bmatrix} R_a & 0 & 0 \\ 0 & R_b & 0 \\ 0 & 0 & R_c \end{bmatrix}. \tag{4}$$

The general force statement for electrical machines could be stated as in Eq. (5):

$$F = \frac{1}{2}i^T\frac{dL(x)}{dx}i. \tag{5}$$

When the mutual inductance of the SRM due to the coupling between the phases is neglected, the induced force by motor F, by rearranging Eq. (5), is as follows:

$$F = \frac{1}{2}\left[i_a^2\frac{dL_{aa}}{dx} + i_b^2\frac{dL_{bb}}{dx} + i_c^2\frac{dL_{cc}}{dx}\right]. \tag{6}$$

An equivalent circuit for a single phase of the LSRM is shown in Figure 4.

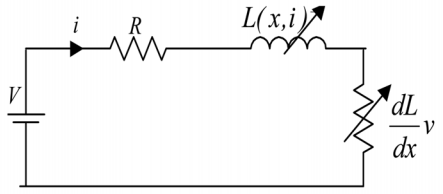

Figure 4. An equivalent circuit for the single phase.

In the LSRM, the motor phase inductance varies depending on the rotor position and the current passing through the coil. The equivalent circuit of the LSRM for a single phase is seen in Figure 4. The calculated dynamic and electrical equations of the motor from this figure includes 2nd degree differentials. To simulate the dynamic behavior of motor using the Euler method or the 4th degree Runge–Kutta method, we need the state space equations from the 3 phases of the motor to be 1st degree. Hence, to degrease the dynamic equations' degrees to the 1st degree, Eqs. (7), (8), and (9) were written.

$$K_{aa} = R_a + v(dL_{aa}/dx) \tag{7}$$

$$K_{bb} = R_b + v(dL_{bb}/dx) \tag{8}$$

$$K_{cc} = R_c + v(dL_{cc}/dx) \tag{9}$$

The LSRM model is not complete without an equation describing the dynamic behavior of the LSRM. The following equations for the translator motion could be written as:

$$T = J\frac{d\omega}{dt} + B\omega + T_L, \tag{10}$$

where F is the motor-induced force, m is the mass of the translator and load, B is the damping coefficient, and F_L is the load force. The state space equation for the dynamics of the LSRM can be obtained, where all of the parameters of the motor are included, in Eq. (11).

$$\begin{bmatrix} v' \\ i'_a \\ i'_b \\ i'_c \end{bmatrix} = \begin{bmatrix} -\frac{B}{m} & 0 & 0 & 0 \\ 0 & -\frac{K_{aa}}{L_{aa}} & 0 & 0 \\ 0 & 0 & -\frac{K_{bb}}{L_{bb}} & 0 \\ 0 & 0 & 0 & -\frac{K_{cc}}{L_{cc}} \end{bmatrix} \begin{bmatrix} v \\ i_a \\ i_b \\ i_c \end{bmatrix} + \begin{bmatrix} \frac{1}{m} & 0 \\ 0 & \frac{1}{L_{aa}} \\ 0 & \frac{1}{L_{bb}} \\ 0 & \frac{1}{L_{cc}} \end{bmatrix} \begin{bmatrix} (F - F_L) \\ V \end{bmatrix} \tag{11}$$

This model does not take into account the effects of the mutual inductances, hysteresis, or eddy-current losses. The accuracy of this model depends on the accurate model of the motor inductance. Hence, the inductances of the motor can be given as follows:

$$L_1 = (L_{\max} + L_{\min})/2, \tag{12}$$

$$L_2 = (L_{\max} - L_{\min})/2, \tag{13}$$

$$L_{aa} = L_1 + L_2 \cos 4x, \tag{14}$$

$$L_{bb} = L_1 + L_2 \cos(4x + 2\pi/3), \tag{15}$$

$$L_{cc} = L_1 + L_2 \cos(4x - 2\pi/3). \tag{16}$$

The variations of the inductances of the 3 phases with an angular position are derived according to the cosine method.

4. Velocity control of the LSRM

In Figure 5, a PI control algorithm is given. In the system, the error after processing is transferred to the output. The error signal $e(t)$ is multiplied by the system gain and then becomes integrated. In the system, the PI control adjusts the output according to the e(t) value. The PI control equation is given in Eq. (17).

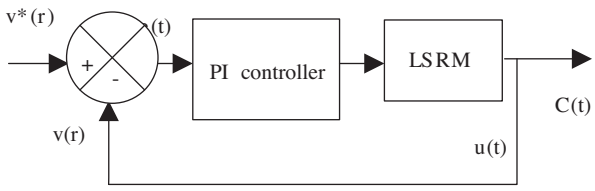

Figure 5. PI control system.

$$u(t) = K_p \left(e(t) + \frac{1}{T_1} \int_0^t e(t)dt \right) \tag{17}$$

The fuzzy logic controller is used to control the velocity of the LSRM. The input variables of the system in the fuzzy logic controller are defined as (e), velocity error, and (ce), change in velocity error. The error and the change in the error obtained are converted into a per unit value. The triangle membership function curves used to calculate the membership values of these values are shown in Figure 6 [7,8]. Figure 6 shows the design of a fuzzy logic controller system. Figure 7 shows the membership values of the fuzzy logic.

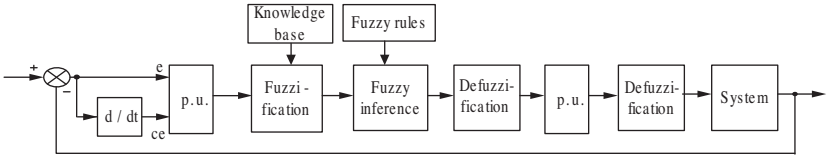

Figure 6. Block diagram design of a fuzzy logic controller system.

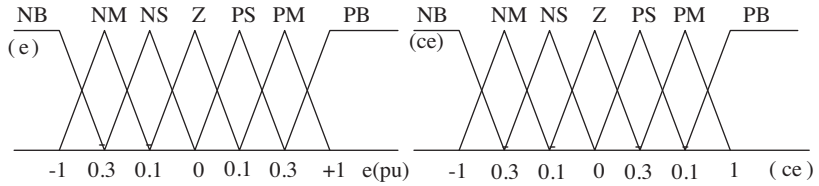

Figure 7. Membership values of the fuzzy logic.

The output of the fuzzy logic is the reference current value of the motor. The velocity of the motor was controlled in this way. The input variables of the system are as follows:

$$\begin{aligned} e(k) &= v_r^*(k) - v_r(k) \\ ce(k) &= e(k) - e(k-1) \end{aligned}, \tag{18}$$

where $e(k)$ is the value of the error at time k, *ce(k)* is the change of the error at time *(k – 1)*, $v_r^*(k)$ is the reference velocity at time k, $v_r(k)$ is the actual velocity at time k, and *(k – 1)* is the error at time *k – 1*. Consequently, the control signal sent to the LSRM can be stated as follows:

$$\begin{aligned} e(pu) &= e(k)/GE \\ ce(pu) &= ce(k)/GC \end{aligned}. \tag{19}$$

The output definition of the fuzzy logic controller is:

$$I_k = I_{(k-1)} + GU * du(pu), \tag{20}$$

where I_k is the controller output value for the kth sampling, $I_{(k-1)}$ is the previous controller output value of the kth sampling, and *GU*du(pu)* is the output reaction for the kth sampling. The obtained value is the reference current value. This reference current value is used to control the velocity of the LSRM.

5. Implementation of the velocity controller

When a translator pole is energized, the motor force is in the direction that will reduce the reluctance. Thus, the nearest rotor pole is pulled from the unaligned position into alignment with the translator field. When the rotor moves to the aligned position, the push/pull force generates the amount of changing reluctance. The current of the phase winding is the other parameter that affects the motor push/pull force. The force is proportional to the square of the current, and so it is an independent current direction. When the sequence of the phase switching is changed, the motion direction of the motor is changed. Therefore, the features of the converter could affect the performance of the motor.

Residual energy in windings is the most important point in designing the driver of the LSRM. If there is residual energy in the windings while the translator is moving towards an unaligned position from the aligned position, a breaking force occurs. To prevent this disadvantage, the winding current must be cut off before the aligned position is reached. Therefore, this cutoff time is defined using the position and speed information of the motor by the PIC microcontroller.

The control block diagram of the LSRM is shown in Figure 8. The position data and current values are sensed by the microcontroller. Depending on this information, the PIC microcontroller produces a pulse-width modulation (PWM) signal for the buck converter power switch and decides the sequence for the phase windings. The PWM signal controls the speed of the motor [29].

The appropriate phase must be energized to the drive motor. The control program that is loaded into the PIC microcontroller decides which power switches must be energized according their positions. The next phase windings are energized with the position data. The reference current level is used for the limitation of the maximum current of the windings. The input values of the PIC microcontroller are the motor position (x) and current value.

The LSRM phase currents are measured as an analog value produced by the current sensors. The analog value increases the microcontroller level (0–5 V) by op-amps. For every phase current measured, one current sensor is used. This analog value is converted to a 10-bit digital value and the phase current is limited to the reference value [29]. A linear incremental sensor is used for sensing the motor position, which produces a square wave pulse per 62.5 μm, as well as 1 reset signal per 0.5 mm. The pulses are sensed on the microcontroller's capture pin (high-speed counter). The reset pulse is sensed by an external interrupt pin with high priority. Thus, the failure of the sensed position is reset every 0.5 mm. In Figure 9, a view of the controller circuit, driver, and controller is shown [29].

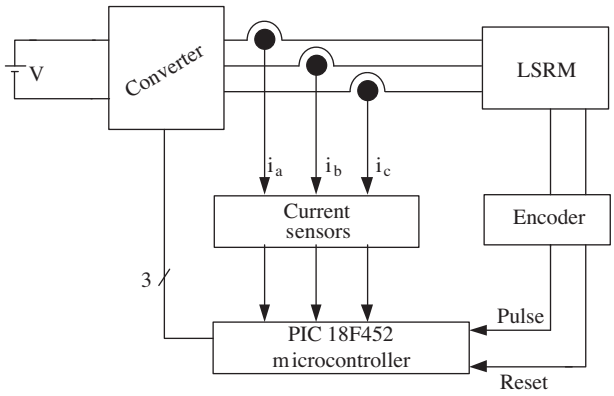

Figure 8. Control block diagram of the LSRM.

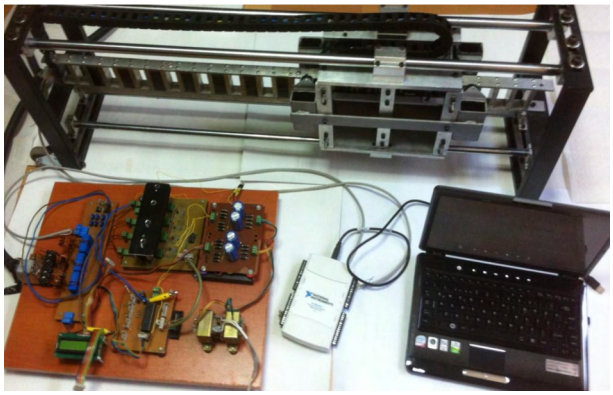

Figure 9. The experimental setup of the LSRM.

6. Simulation results

The LSRM used for the simulation has 3 phases, 6/4 poles, 8 A, 24 V, 250 W, 1 m/s nominal velocity, B = 0.0012 coefficient of friction, and m = 25 kg mass of the translator. In the simulation, the common transfer velocity and the transfer angle are set as 0–50 and 150, respectively. The velocity of the LSRM is controlled using the fuzzy logic and PI control methods. The switching angle of the phase currents is arranged on the basis that no negative force will be produced.

The switching zones of the phase currents and strategies are determined according to the translator position of the motor from the inductance curve obtained in Figure 3. The 3 phase currents of the LSRM are calculated using the 4th degree Runge–Kutta method. In the simulation, the motor is not fully loaded and its current is not at the maximum value.

First, a 1 m/s constant reference velocity is determined. Next, the motor is controlled using the PI control method. The values of k_i and k_p that are used in the PI control are 1 and 62, respectively. The PI control parameters are found (selected) using the Ziegler–Nichols method. As can be seen in Figure 10, the motor reaches a 1 m/s velocity at a distance of about 8 mm. Thus, it performs an acceleration movement at between 0 and 8 mm. The motor then moves at a 1 m/s constant velocity up to 100 mm. The motor reaches a 1 m/s velocity at about 6 mm when the FLC algorithm is used. Figure 10 shows the velocity curves of the LSRM with the PI control and FLC.

It can be seen that the response of the FLC is closer to the reference velocity than that of the PI method, and that the curve obtained by the FLC method reaches the reference velocity more quickly than the curve obtained with the PI method. In Figure 11, we can see the velocity error curves of the translator with the PI and FLC methods. The velocity error direction is negative in the PI control, while the velocity error is positive in the FLC. Although the velocity errors are very small values, the velocity error in the FLC is smaller than that in the PI control. Figure 12a shows the phase currents of the LSRM accelerating with the PI control; Figure 12b shows the phase currents with the FLC. The currents move at a 1 m/s constant velocity with a constant 25 N load during the movement from the starting point to 100 mm. Because of the translator velocity, more than reference velocity at 25 N loads, the motor phase currents are lower than the maximum current. Thus, there is no current chopping. When the real velocity of the translator is more than the reference velocity, the switches are cut off in order to force the translator velocity to the reference value. The velocity signals are also recorded while the motor is loaded with the load changing conditions, as shown in Figure 13.

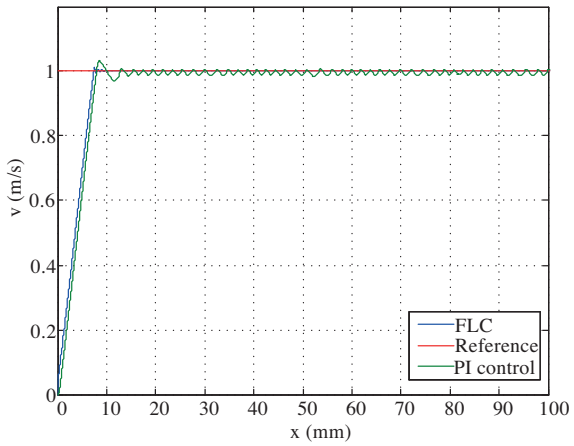

Figure 10. Velocity curves of the translator with PI control and FLC.

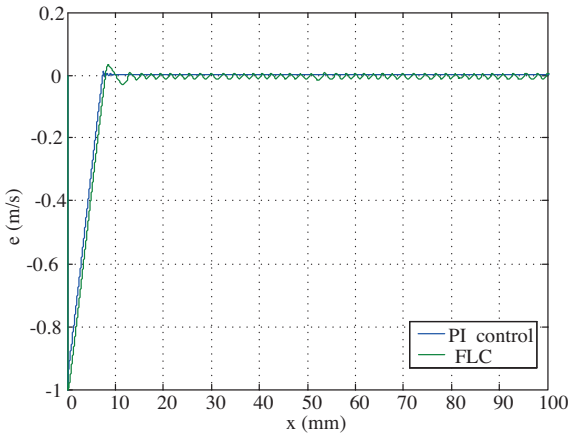

Figure 11. Velocity error curves of the translator with the PI control and FLC.

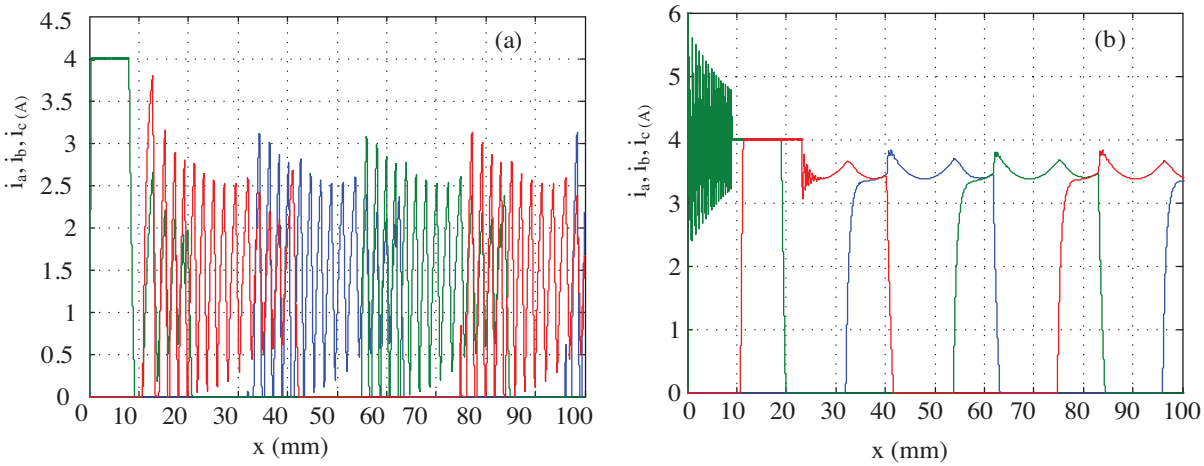

Figure 12. Motor phase currents accelerating with a) PI control and b) FLC.

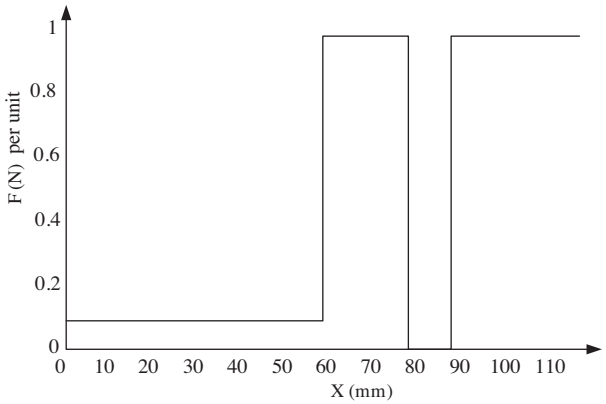

Figure 13. Motor load changing with the PI control and FLC.

The velocity curves of the translator under increased load conditions with the PI control and FLC are shown in Figure 14. The load attachment to the translator is initially done as 25 N between 0 mm and 60 mm. It is 250 N between 60 mm and 80 mm. In the positions between 80 mm and 90 mm, the load is removed. In the last stage, the motor is reloaded with 250 N between 90 mm and 100 mm.

Within the reference velocity, the performance of the translator is observed under load with the PI control and FLC methods shown in Figure 14. As can be seen, the performance of the FLC is better than that of the PI control. While the PI control algorithm catches the reference velocity at about 7.8 mm, the FL control catches the reference velocity at about 8 mm. In addition, the velocity error curves of the PI and FLC algorithms with the above test conditions are shown in Figure 14, where the error of the FLC strategy at a steady state is very close to zero, even when the motor is heavily loaded. Figure 15 shows the contrary position velocity error curves of the translator under load with PI control and FLC. We can see the error curves of the translator by speeding up the loaded motor with the PI and FLC. If we examine the data separately, the motor reaches the reference velocity at about 8 mm.

Figure 16 shows the phase currents of the LSRM during speeding up and the response of the load changing. The motor is started with 25 N loads and it reaches a 1 m/s constant velocity at 8 mm. While running at this constant velocity, at 60 mm, the load is increased to 250 N, and then at 80 mm, the load is completely unloaded. Next, at 90 mm, the motor is reloaded with 250 N. There is chopping in the motor phase currents

after the motor velocity reaches the reference value and while the motor is unloaded. The steady state current value of the motor with the unloaded condition is lower with the PI control than that of the condition with the 25 N load, as shown in Figure 16a. However, the steady state current value of the motor with the unloaded condition is lower with FLC than that of the condition with the 25 N load, as shown in Figure 16b. As a result, with the PI control method, if the motor loaded with 250 N is running with a 25 N load, the occurring velocity error is smaller than if it is loaded with same load but with no load running. It can be said that if the motor is loaded instantly with any load, the FLC method is sufficient, but the PI control method is insufficient. As a result, we can say that, electromechanically, the fluctuations in the current mean a fluctuation in the force. In this respect, the FLC response is better than that of PI control.

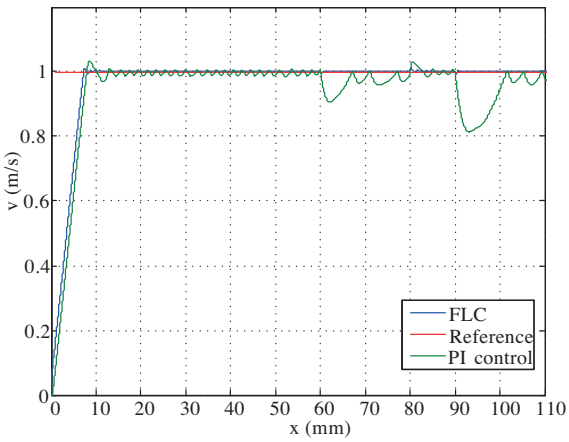

Figure 14. Velocity curves of the translator under load with PI control and FLC.

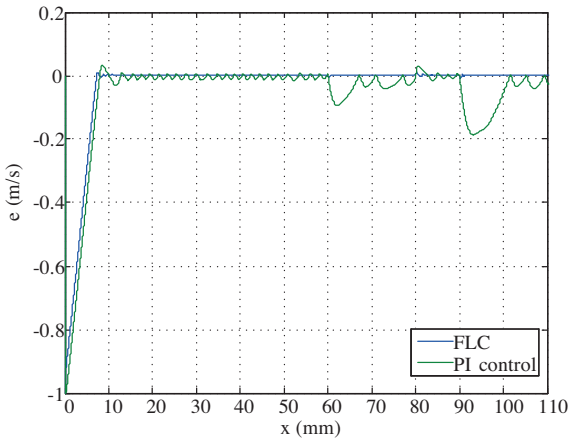

Figure 15. Velocity error curves of the translator under load with PI control and FLC.

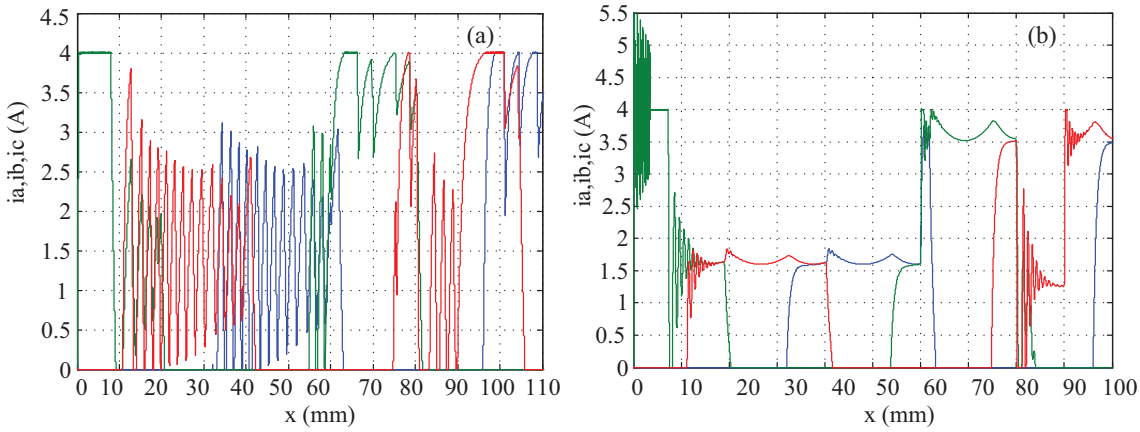

Figure 16. Motor phase currents versus position accelerating with a) PI control and b) FLC.

7. Experimental results

The inductance data of the designed motor are collected with the finite element method (FEM) using the Maxwell Ansoft program. Moreover, the simulation of the inductance curves of the 3 phases is released. In the simulations, we use the cosine method. We draw an inductance curve for phase A with the normalized data in Figure 17. We compare the drawing with the experimental data and calculate it using the FEM. As a result, both of these graphs are very similar, and we use the cosine method because it is easier than the other methods. The dynamic equations of the LSRM are obtained from this inductance profile.

It can be seen from Figures 18a and 18b that the currents of the motor phase are in scope view. In the simulation phase, the currents are triggered with a sequence and do not start before a phase current unless the 3rd phased current is finished. This can be seen in the scope view.

In Figure 19, the graph is drawn using the experimental data. The data are collected using a data acquisition board, drawn using Microsoft Excel, and saved using the LABVIEW program.

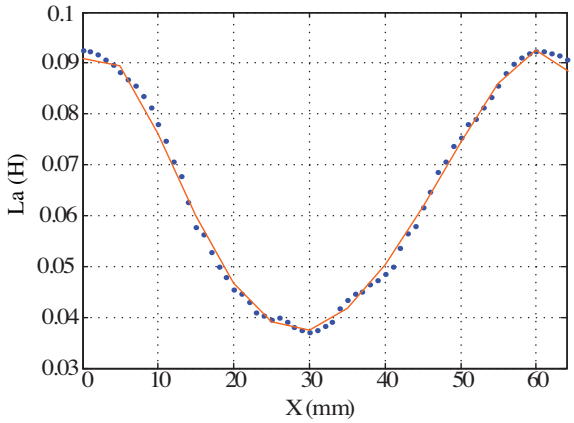

Figure 17. Motor one-phase inductance graphic data obtained by the FEM method and LABVIEW.

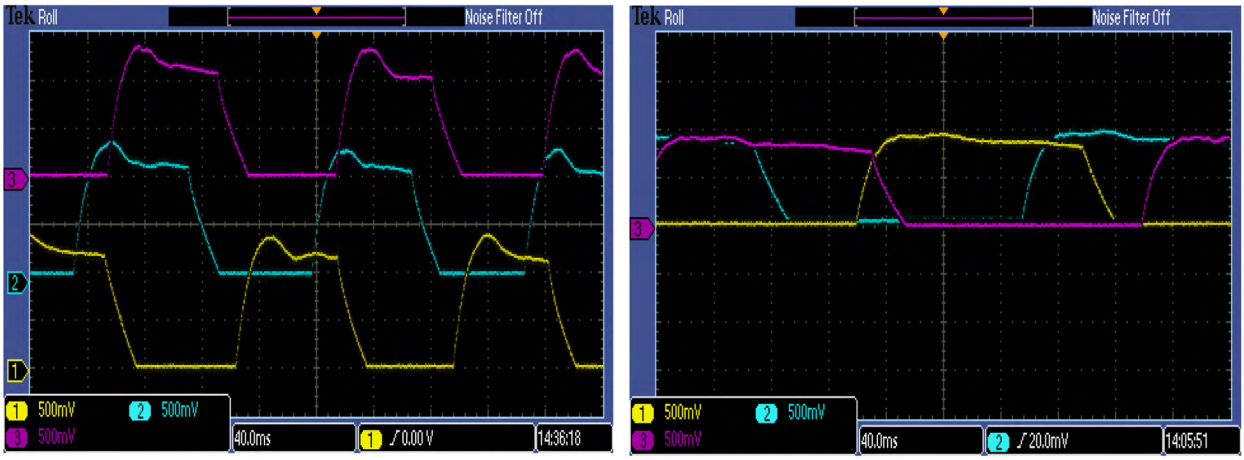

Figure 18. The different currents of the phases in scope view.

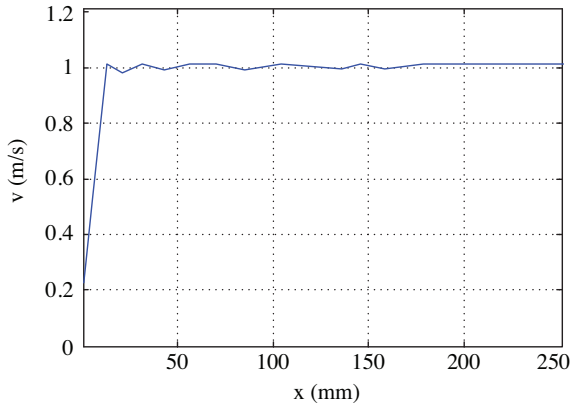

Figure 19. The shapes and the display outputs of the velocity and position obtained by LABVIEW with FLC.

8. Conclusion

In this study, the velocity response of the PI- and fuzzy logic-controlled double-sided LSRM was simulated and experimented. The simulated motor has 6/4 poled, 3-phase, 250 W power. The PI and fuzzy logic velocity responses of the motor were compared according to the determined values, and it was observed that FLC is more useful than the PI control method.

It was concluded from the obtained simulation results that the motor may be used where linear motion is needed in places such as elevators, hospitals, and subway doors and where accurate position control and rapid response are required, due to their low cost, high efficiency, and high rate of force/volume.

Acknowledgment

This study was supervised and supported by the 00401.STZ.2009 - 1 coded SANTEZ project by the Republic of Turkey Ministry of Science, Industry, and Technology with the EMSA Automation Trade Cooperation and Gazi University.

References

[1] P.K. Budig, "The application of linear motors," Proceedings of the 3rd IEEE International Power Electronics and Motion Control Conference, Vol. 3, pp. 1336–1341, 2000.

[2] H.S. Lim, R. Krishnan, "Ropeless elevator with linear switched reluctance motor drive actuation systems", IEEE Transactions on Industrial Electronics, Vol. 54, pp. 2209–2218, 2007.

[3] S.W. Zhao, N.C. Cheung, W. Gan, J.M. Yang, J.F. Pan, "A self-tuning regulator for the high precision position control of a linear switched reluctance motor", IEEE Transactions on Industrial Electronics, Vol. 54, pp. 2425–2434, 2007.

[4] T.J.E. Miller, Switched Reluctance Motors and Their Control, New York, Oxford University Press, 1993.

[5] M. Dursun, H. Özbay, F. Koç, "An elevator driver with linear motor", Elevator Symposium, İzmir, Turkey, pp. 233–239, 2010 (in Turkish).

[6] M. Dursun, F. Koc, H. Özbay, "Determination of geometric dimensions of a double sided linear switched reluctance motor", World Academy of Science, Engineering and Technology, Vol. 6, pp. 32–38, 2010.

[7] M. Dursun, F. Koç, "Simulation of fuzzy logic position and speed control of double sided linear switched reluctance motor", International Conference on Modeling, Simulation and Control, pp. 517–521, 2010.

[8] M. Dursun, "Estimation of passenger waiting time in elevator system with artificial neural network", Intelligent Automation and Soft Computing, Vol. 16, pp. 101–110, 2010.

[9] M. Dursun, "A wheelchair design driven with fuzzy logic controlled switched reluctance motor supplied by PV arrays", Journal of Applied Science, Vol. 8, pp. 3351–3360, 2008.

[10] Y.J. Liu, G.P. Widdowson, S.Y. Ho, W.C. Gan, P. Borsje, "Design and analysis of linear switched reluctance motor for high precision position control", International Conference on Electrical Machines and Systems, Vol. 1, pp. 55–58, 2007.

[11] M. Dursun, F. Koç, H. Özbay, S. Özden, "Design of linear switched reluctance motor driver for automatic door application", International Conference on Information and Industrial Electronics, Vol. 2, pp. 424–427, 2011.

[12] M. Dursun, F. Koç, "Simulation of velocity control of linear switched reluctance motor", International Conference on Computer Engineering and Technology, pp. 367–372, 2011.

[13] F. Daldaban, N. Üstkoyuncu, "A new double sided linear switched reluctance motor with low cost", Energy Conversion and Management, Vol. 47, pp. 2983–2990, 2006.

[14] S.W. Zhao, N.C. Cheung, "Trajectory control of a linear switched reluctance motor using a two-degree-of-freedom controller", First International Power and Energy Conference, pp. 492–496, 2006.

[15] M. Dursun, S. Özden, "PC based data acquisition system for PLC controlled linear switched reluctance motor", Turkish Journal of Electrical Engineering & Computer Sciences, Vol. 21, pp. 71–80, 2013.

[16] M. Dursun, H. Özbay, "Design and analysis of a double sided linear switch reluctance motor driver for elevator door", Przeglad Elektrotechniczny, Vol. 87, pp. 293–296, 2011.

[17] A. Fenercioğlu, M. Dursun, "Design and magnetic analysis of a double sided linear switched reluctance motor", Przeglad Elektrotechniczny, Vol. 86, pp. 78–82, 2010.

[18] M. Dursun, A. Saygın, "Fuzzy logic controlled switched reluctance motor driver designing for a lift system", Pamukkale University Engineering Faculty Journal of Engineering Sciences, Vol. 12, pp. 151–160, 2006.

[19] M. Dursun, A. Fenercioğlu, "Velocity control of linear switched reluctance motor for prototype elevator load", Przeglad Elektrotechniczny, Vol. 87, pp. 209–214, 2011.

[20] H.S. Lim, R. Krishnan, N.S. Lobo, "Design and control of a linear propulsion system for an elevator using linear switched reluctance motor drives", IEEE Transactions on Industrial Electronics, Vol. 55, pp. 534–542, 2008.

[21] X. Liu, Y.Y. Ye, Z. Zheng, "A novel tubular permanent magnet linear synchronous motor used for elevator door", International Conference on Electrical Machines and Systems, Vol. 1, pp. 1277–1280, 2007.

[22] H.K. Bae, B.S. Lee., P. Vijayraghavan, "A linear switched reluctance motor: converter and control", IEEE Transactions on Industry Applications, Vol. 36, pp. 1351–1359, 2000.

[23] J.G. Amoros, P. Andrada, B. Blanque, "An analytical approach to the thermal design of a double-sided linear switched reluctance motor", 19th International Conference on Electrical Machines, pp. 1–4, 2010.

[24] U.S. Deshpande, J.J. Cathey, E. Richter, "A high force density linear switched reluctance machine", IEEE Transactions on Industry Applications, Vol. 31, pp. 345–352, 1995.

[25] B.S. Lee, H.K. Bae, P. Vijayraghavan, R. Krishnan, "Design of a linear switched reluctance motor", IEEE Transactions on Industry Applications, Vol. 36, pp. 1571–1580, 2000.

[26] J.M. Yang, H.P. Li, X. Jin, J. Liu, S.W. Zhao, Q. Zhong, N.C. Cheung, "Passivity-based control of linear switched reluctance motors", Proceedings of the Institution of Mechanical Engineers, Part I: Journal of Systems and Control Engineering, Vol. 223, pp. 1027–1034, 2009.

[27] H.Y. Li, Y.L. Liu, J. Wang, Y.K. Wong, W.L. Chan, "Neural network based nonlinear H(infinity) control for linear switched reluctance motor", 7th Asian Control Conference, Vol. 1–3, pp. 796–801, 2009.

[28] H. Chen, X. Qiu, Y. Zhao, "Conductive EMI noise measurement for switched reluctance drive", Turkish Journal of Electrical Engineering & Computer Sciences, Vol. 17, pp. 253–259, 2009.

[29] F. Koç, "Position control of linear switch reluctance motor," MSc Thesis, Department of Electrical Education, Institute of Science and Technology, Gazi University, Ankara, Turkey, 2011.